

MUVO: A Multimodal Generative World Model for Autonomous Driving with Geometric Representations

Daniel Bogdoll* and Yitian Yang* and J. Marius Zöllner

FZI Research Center for Information Technology

KIT Karlsruhe Institute of Technology

bogdoll@fzi.de

Abstract

Learning unsupervised world models for autonomous driving has the potential to improve the reasoning capabilities of today’s systems dramatically. However, most work neglects the physical attributes of the world and focuses on sensor data alone. We propose MUVO, a MULTimodal World Model with Geometric VOxel Representations to address this challenge. We utilize raw camera and lidar data to learn a sensor-agnostic geometric representation of the world, which can directly be used by downstream tasks, such as planning. We demonstrate multimodal future predictions and show that our geometric representation improves the prediction quality of both camera images and lidar point clouds. The code and model weights are available at GitHub.

1. Introduction

From a young age, humans continuously observe and engage with the world, constructing an understanding of the environment. As a result, we can intuitively understand scenes from and predict potential changes therein. For autonomous vehicles, reasoning about a scene and predicting multiple plausible futures is crucial to navigating our complex and highly interactive world. To achieve this, recently, action-conditioned generative world models have emerged, which learn a compact representation of the world and predict future states [29, 30]. However, a majority of existing world models take RGB images as input [40, 41] and operate in simple environments [31, 32], rendering them ill-equipped for the complex task of autonomous driving.

We leverage the abundance of unlabeled sensor data collected by autonomous vehicle fleets. Our world model takes raw, high-resolution camera images and lidar point clouds as inputs and predicts multimodal future observations conditioned on actions. To equip our model with a more pro-

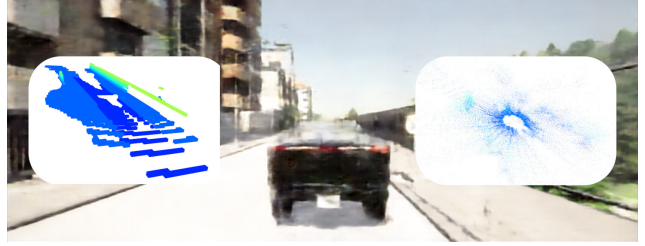


Figure 1. This example shows a high-resolution future prediction from MUVO for 3D occupancy and camera and lidar observations.

found environmental understanding, we also learn a sensor-agnostic 3D geometric representation of the world.

Our contributions can be summarized as follows:

- A novel unsupervised generative world model that leverages multimodal sensor setups of autonomous vehicles and predicts future predictions for both camera and lidar.
- A novel approach to learning a sensor-agnostic, actionable environment representation for world models in the form of a 3D geometric voxel occupancy representation.
- A novel approach for action-conditioned 3D Occupancy Prediction, expanding the state-of-the-art.

2. Related Work

2.1. World Models

World models are generative models that embed observations into latent states, predict future states conditioned on actions, and decode these latent predictions into the observation space [4, 54]. World models originate from reinforcement learning, where they are mostly used as neural simulators to reduce environment interactions. Many approaches use simple, low-resolution simulation environments [2, 25, 29–32, 34, 38, 48, 51, 74, 85, 90].

However, advancements have been made in complex environments and with real-world data. However, several approaches rely on labels, privileged information, or expert-designed state spaces, limiting their ability to scale.

*These authors contributed equally

MILE [40] and SEM2 [26] predict semantic labels in the Bird’s-Eye-View (BEV) based on supervision during training in simulation. DriveDreamer [106] conditions real-world RGB images on HD maps and labeled 3D bounding boxes. Based on a diffusion model [83], future frames and actions in the form of yaw angle and velocity are jointly predicted. The style of predictions is guided by CLIP [80] embeddings, using annotated scenes during training. SWIM [69] learns how human hands interact with their environment based on an expert-designed action space. A detector trained on labeled data is leveraged to derive actions from unlabeled real-world videos. TrafficBots [132] formulates traffic simulation as a world model by learning a multi-agent policy from real-world data, relying on privileged information and expert-designed states.

There also exist unsupervised world models. DreamerV3 is capable of predicting plausible futures in Minecraft [33]. DriveGAN [52] was trained on real-world data and acts as an action-conditioned neural simulator. DayDreamer [32, 112] learns robotic tasks from real-world visual inputs. A world model from Tesla [23], trained on proprietary real-world multi-camera RGB data, was demonstrated to predict future observations and semantic or geometric data based on supervised fine-tuning.

Following a recent line of work interpreting world models as a single sequence model [12, 17, 45, 63, 71, 81, 113], GAIA-1 [41] was trained on proprietary real-world camera data and can be conditioned with both actions and textual inputs. Vector quantization [99] was used to tokenize the data. Based on a video diffusion decoder, it achieved temporally consistent, high-resolution predictions. Following a similar approach, Zhang et al. presented a world model for real-world lidar point clouds [129]. Instead of actual actions, they utilize ego vehicle poses.

2.2. Sensor Fusion

Fusion approaches in autonomous driving typically use camera and lidar sensors. Recently, a shift towards transformer-based [43, 100] architectures can be observed. There are multiple works [46, 61, 66, 67, 128] who perform camera-lidar fusion on the BEV level [78]. Others improve upon this by utilizing 3D voxel features [57, 133]. Sparse representations [7, 56, 115], modality interactions, and intermediate fusions are becoming more common [15, 64, 118, 124]. While many works deal with robustness against lidar failures, dealing with inferior image conditions is underrepresented [1]. Other works focus on interpretability [86], real-time performance [77], event streams [103], modality agnosticity [14], or auxiliary supervision [79].

2.3. 3D Occupancy

While 2D BEV grids are common in autonomous driving, they cannot fully capture the environment. 3D occupancy is

a ”geometric-aware representation of the scene” [92].

Data. The most common dataset that provides semantic voxels for occupancy mapping and scene completion is SemanticKITTI [3, 27]. More recently, further small occupancy datasets [58, 65, 92, 98, 107] were released, providing voxel data for further datasets [5, 62, 94, 114]. The only large-scale benchmark is OpenScene [18], based on nuPlan [6]. Dense ground truth for voxels is typically derived from multiple lidar point clouds.

Scene Completion. For camera-based inputs, MonoScene [8] was the first work to infer 3D semantic voxels from a single 2D camera image, reconstructing visible areas and hallucinating occluded ones. Transformer-based architectures [59, 130] have improved upon their results using sparse representations or hybrid encoders. Symphonies [47] leverages instance queries to model relations between pixels and voxels that belong to the same instance. Recent approaches introduce zero-shot open-vocabulary occupancy segmentation, eliminating the need for supervision [95, 101]. Novel works often leverage multi-camera setups. OccDepth [70] uses stereo cameras to derive depth, while many others [22, 44, 60, 102, 108, 110] utilize four or more cameras for surround vision. Finally, also methods based on lidar point clouds exist [82, 93, 119].

Instead of relying on 3D supervision, recent works [9, 75, 76, 111] utilize multi-view 2D neural rendering to create voxel-based 3D meshes. CLONer [10] uses a single camera and lidar frame as inputs to predict occupancy grids based on neural rendering. S4C [35] predicts semantic occupancy from a single image, relying on supervision.

Lidar Perception. Many state-of-the-art methods voxelize point clouds to derive features. VoxelNet [134] is a popular Voxel Feature Extractor (VFE) often used [121, 126, 135, 136]. Here, all lidar points are grouped into voxels first to obtain point- and then voxel-wise features. Recently, more efficient encoders and methods have emerged to utilize voxel representations [19, 28, 42, 53, 87, 88, 91, 96, 105, 116, 125]. Voxel representations are also common in transformer-based architectures [24, 57, 68, 104, 122].

Pre-Training. Multiple methods [39, 73, 117] perform voxelwise masking [37] on point clouds. UniPAD [123] masks point clouds or multi-view images, projects them into voxels, and utilizes neural rendering for reconstructions. SPOT [120] relies on supervision for semantic occupancy prediction for lidar point clouds. UniScene [72] utilizes multi-view images to predict 3D Occupancy.

Forecasting. The OpenOcc benchmark [92] Was the first to include voxelwise flow information, similar to OpenScene [18]. A occupancy network by Tesla was demonstrated to predict motion flow vectors for voxels [22]. Khurana et al. combine lidar data with motion sensors to predict future 3D occupancy [50]. Liu et al. introduced the task of Occupancy Completion and Forecasting, where they predict

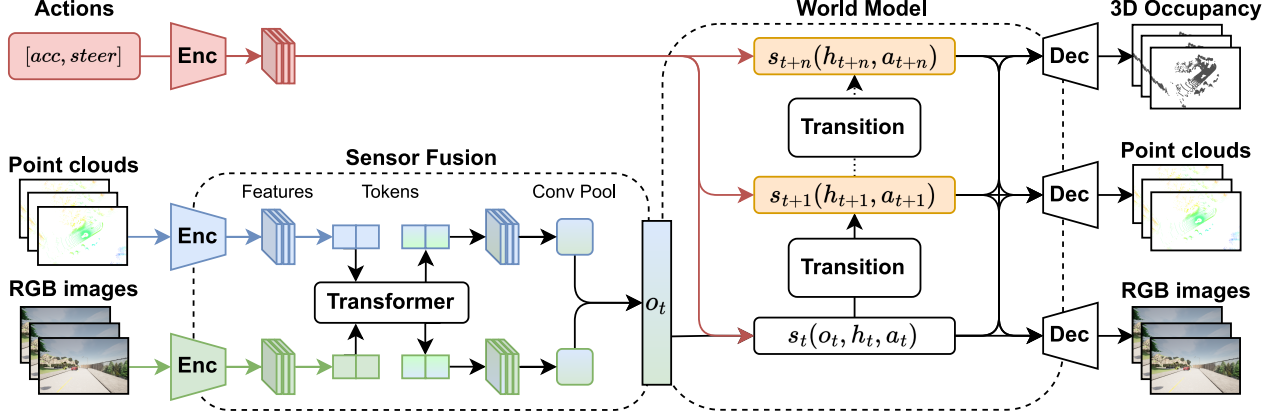


Figure 2. **Overview of MUVO.** Our model consists of three stages, from left to right. First, raw camera images and lidar point clouds are processed, encoded, and fused. The resulting latent representations are then fed into our transition model. Conditioned on actions, future states are predicted. Finally, we decode these future states into 3D occupancy grids, raw point clouds, and raw RGB images.

dense 3D occupancy voxels [65]. Similarly, UniWorld [13] utilizes multi-view images to forecast 3D occupancy.

3. Method

In this work, we propose MUVO, a **M**ultimodal **W**orld **M**odel with Geometric **V**oxel **R**epresentations. Our model utilizes high-resolution image and lidar sensor data from an autonomous vehicle to predict raw camera and lidar data as well as 3D occupancy representations multiple steps into the future, conditioned on actions.

Our model consists of three stages, as shown in Figure 2. First, we process, encode, and fuse high-resolution RGB camera data and lidar point clouds with a transformer-based architecture. Second, we feed the latent representations of the sensor data to a transition model to derive a probabilistic model of the current state, followed by sampling, while concurrently predicting the probabilistic model of future states and sampling from it. Lastly, we decode both current and future states from the probabilistic models, forecasting raw RGB images, point clouds, and 3D occupancy grids multiple frames into the future.

We argue that prior world models primarily learn patterns in the data rather than modeling the real world [97]. Our unsupervised approach to learning sensor-independent geometric occupancy representations provides the model with an underlying understanding of the physical world.

3.1. Observation Encoder

Input representations. Prior multimodal world models [90, 112] were based on low-resolution inputs, unable to capture relevant details in driving scenes [15, 40]. Contrary, our model builds upon a typical sensor setup of autonomous vehicles comprising stereo cameras and lidar [27, 109]. We utilize RGB images from a front camera and point clouds

from a top-mounted lidar as inputs for our network. For the task of multimodal world modeling, we found bijective, lossless range view representations for lidar point clouds most effective, see Sec. 5. In addition, they show computational advantages over voxel-based methods [24]. The 3D point cloud, comprising up to 60,000 points with coordinates (x, y, z) , is projected into a 2D cylindrical projection $\mathcal{R}(u, v)$ with dimensions $H_r \times W_r$:

$$\begin{pmatrix} u \\ v \end{pmatrix} = \begin{pmatrix} \frac{1}{2} (1 - \arctan(y, x) \pi^{-1} W_r) \\ (1 - (\arcsin(z, r^{-1}) + |f_{\text{down}}|) f_v^{-1}) H_r \end{pmatrix} \quad (1)$$

where (u, v) represent the coordinates of each point in the 2D range view image. Each projected point’s coordinates (x, y, z) and range r are stacked along the dimension axis to form (x, y, z, r) , as features of each projected point in the 2D range view image, leading to $\mathcal{R}(u, v) \in \mathbb{R}^{4 \times H \times W}$. For pixels where no points are projected, the coordinates (x, y, z) are set to 0, and r is assigned a value of -1 , effectively indicating the absence of data at these coordinates.

For images $\mathcal{I} \in \mathbb{R}^{3 \times H_i \times W_i}$, we adopt the recommendations of Hu et al [40]. Our model takes images of resolution 600×960 pixels as input. Subsequently, we perform minor cropping to exclude irrelevant areas, such as the sky.

Encoder. For the image data $\mathcal{I} \in \mathbb{R}^{3 \times H_i \times W_i}$ and the point cloud data $\mathcal{R} \in \mathbb{R}^{4 \times H_r \times W_r}$ in range view representation we utilize a pre-trained ResNet-18 [36] as the backbone for feature extraction. We derive multiple feature maps from different ResNet layers with low resolutions similar to [40]. These feature maps are then fused using convolutional layers coupled with either upsampling or downsampling techniques, culminating in the final image features $\mathcal{F}_c \in \mathbb{R}^{C \times H_c \times W_c}$ and point cloud features $\mathcal{F}_L \in \mathbb{R}^{C \times H_L \times W_L}$. These encoded representations are then fed into the sensor fusion component.

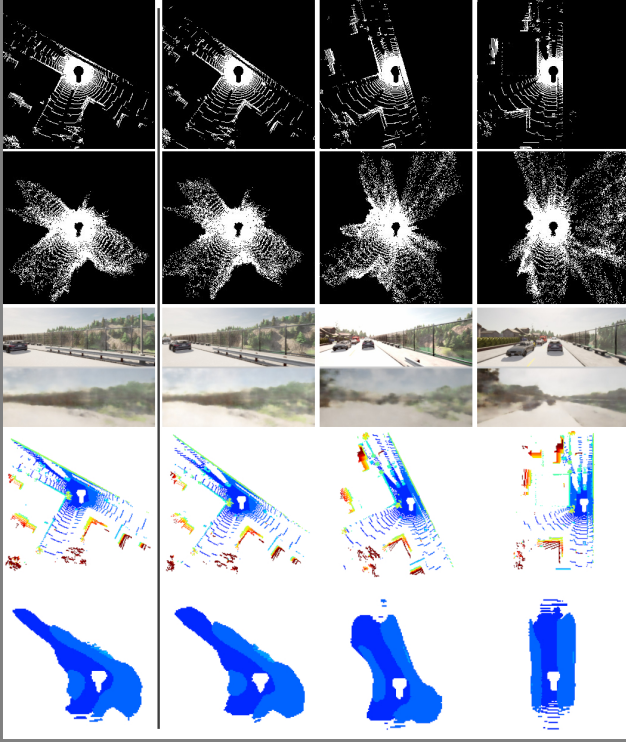


Figure 3. **Predictions for lidar, camera, and 3D occupancy.** Given multiple past frames - represented by the final frame in the left column - we show action-conditioned future predictions for 0.2s, 0.8s, and 1.8s. The top row of each modality shows the ground truth, while the bottom row shows decoded observations.

3.2. Multi-Modal Fusion

Prior multimodal world models relied on naive fusion approaches [26, 90, 112]. Our experiments show that a transformer-based architecture is superior to such naive approaches for the task of prediction, see Sec. 5. Inspired by recent works [15, 21, 86], we employ the self-attention mechanism of a Transformer [100] architecture to fuse features of different sensors. The transformer accepts a sequence of tokens as input, where each token is a D_t -dimensional feature vector, so the required input sequence is $\mathbf{t}_{in} \in \mathbb{R}^{D_t \times N_t}$, with D_t representing the feature dimension of each token and N_t the number of tokens in the sequence. Initially, we flatten the H and W dimensions of the features \mathcal{F} obtained from the encoder described in Sec. 3.1, resulting in tokens $\mathbf{f} \in \mathbb{R}^{C \times HW}$ to match the Transformer’s input shape requirements. Subsequently, we incorporate the 2D sinusoidal positional embedding [15, 100] $\mathbf{e} \in \mathbb{R}^{C \times HW}$ into each token to introduce spatial inductive biases. Additionally, the learnable sensor embeddings $\mathbf{s} \in \mathbb{R}^{C \times N_s}$ are added to each token, introducing a sensor category, where $N_s = 2$ is the number of sensors. The resultant tokens $\mathbf{t} \in \mathbb{R}^{C \times HW}$ are obtained, with each token $\mathbf{t}_i(x, y) =$

$\mathbf{f}_i(x, y) + \mathbf{e}_i(x, y) + \mathbf{s}_i$, where i indicates the i -th sensor, and (x, y) denotes the coordinate index of that token within the sensor feature. These tokens from all sensors are then concatenated and fed into a Transformer encoder comprising k layers, each consisting of multi-head self-attention, MLPs, and layer normalizations, resulting in new tokens $\mathbf{t}_{new} \in \mathbb{R}^{C \times HW}$. These new tokens are reshaped back into the shape of the original input features after backbone, namely $\mathcal{F}_c^{new} \in \mathbb{R}^{C \times H_c \times W_c}$ and $\mathcal{F}_L^{new} \in \mathbb{R}^{C \times H_L \times W_L}$. Each is then subjected to convolutional layers for down-sampling, followed by pooling layers to get 1D features $\mathbf{f}_d \in \mathbb{R}^D$. These two feature vectors, along with 1D features derived from provided route maps and speed information, are processed through convolution layers, MLP, and a pooling layer and subsequently concatenated. This concatenated feature vector is then passed through fully connected layers to reduce its dimensionality, producing the one-dimensional vector $\mathbf{o}_t \in \mathbb{R}^D$ that is fed into the transition model.

3.3. Transition Model

While recent work formulates world modeling as a single sequence model [41, 129], these approaches are computationally intensive. For a more lightweight model, we adopt the fundamental architectures found in MILE [40] and Dreamer [30, 31]. The input consists of fused observation features $\mathbf{o}_{0:t}$ and encoded actions $\mathbf{a}_{0:t} \in \mathbb{R}^{T \times D_a}$, based on a simple MLP, assuming access to a policy or motion planner. The output includes hidden states $\mathbf{s}_{0:t} \in \mathbb{R}^{T \times D_s}$ and deterministic historical states $\mathbf{h}_{0:t} \in \mathbb{R}^{T \times D_h}$, predictions for future states $\mathbf{s}_{t:t+n}$, and $\mathbf{h}_{t:t+n}$, T represents the number of frames, also referred to as the sequence length, and D_a , D_s , D_h are the dimensions of each vector respectively. The deterministic historical variable $\mathbf{h}_{t+1} = f_\theta(\mathbf{h}_t, \mathbf{s}_t)$ is modelled by a Gated Recurrent Unit (GRU) [16] f_θ , enabling the model to remember past states. The posterior hidden state probability distribution is given by $q(\mathbf{s}_t | \mathbf{o}_{\leq t}, \mathbf{a}_{< t}) \sim \mathcal{N}_\phi(\mathbf{o}_t, \mathbf{h}_t, \mathbf{a}_t)$, while the prior hidden state probability distribution, without the input of observed feature \mathbf{o}_t , is given by $p(\mathbf{s}_t | \mathbf{h}_t, \mathbf{a}_{t-1}) \sim \mathcal{N}_\theta(\mathbf{h}_t, \mathbf{a}_{t-1})$. Here, \mathcal{N}_ϕ and \mathcal{N}_θ are probability models modelled by a MLP. Finally, in the presence of observations, \mathbf{s}_t is sampled from the posterior distribution q . while in the absence of observations, i.e., during prediction, $\hat{\mathbf{s}}_t$ is sampled from the prior distribution p .

3.4. Multi-Modal Decoder

Prior world models decode into either abstract representations [26, 40], camera [33, 41], or lidar [129] data. Our model not only decodes into high-resolution camera and lidar data but also a sensor-agnostic 3D occupancy representation, representing the geometrical properties of the physical world. The input for our decoders is a latent dynamic state $(\mathbf{s}_t, \mathbf{h}_t)$ with shape $D_t = D_s + D_h$ which is provided by the transition model.

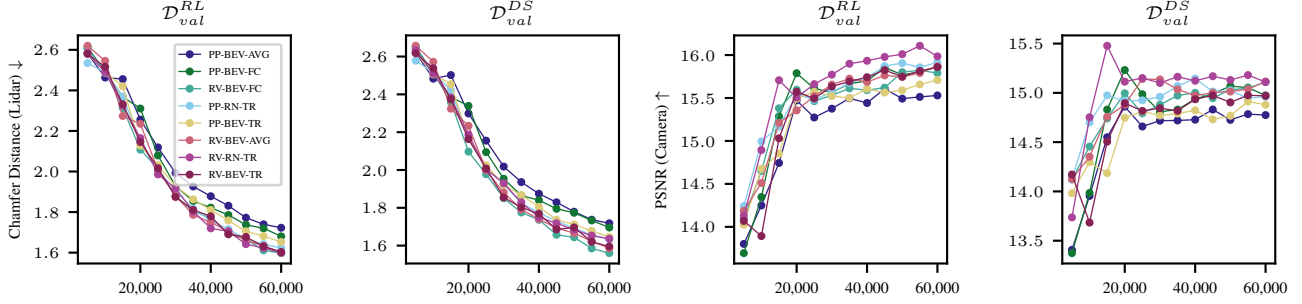


Figure 4. Evaluation of sensor fusion approaches on two validation sets. With \mathcal{D}_{val}^{RL} we evaluate representation learning capacities, while \mathcal{D}_{val}^{DS} examines robustness under domain shifts. For lidar encodings, we evaluated PointPillars (PP) [53] and a range view (RV) [55] representation followed by a ResNet [36]. For camera, we evaluated BEV mapping [78] and a simple ResNet (RN) encoding. For the fusion, we examined feature averaging (AVG) [11], feature concatenation (FC) [112], and a transformer-based architecture (TR) [15].

2D Decoder. As we decode RGB images and point clouds into 2D representations of shape $C \times H \times W$, we are able to use the same decoder architecture for both, since our range view representation of lidar point clouds is loss-less and allows for a direct translation into 3D.

First, the input is reshaped to $D_t \times 1 \times 1$, followed by a convolutional decoder using a kernel $\mathcal{K} \in \mathbb{R}^{H_0 \times W_0}$, where H_0 and W_0 are determined by the final output resolution $H \times W$, to yield an initial 2D feature of dimensions $C_0 \times H_0 \times W_0$. Subsequently, we perform upscaling with convolutional networks similar to [29, 31] to produce a feature map of size $C_n \times H \times W$. For both camera and lidar, we utilize adapted kernels and heads.

3D Decoder. Next to sensor data, we also decode into geometric 3D occupancy voxels. Prior work [50, 65] has explored the field inspired by data-driven video prediction. Contrarily, our approach predicts 3D occupancy conditioned on actions, inherently leveraging a better understanding of the dynamics of the world. Inspired by [40, 49], we decode into 3D instead of 2D. The approach uses a learnable tensor $\mathcal{T}_0 \in \mathbb{R}^{C \times X \times Y \times Z}$, where the tensor size $X \times Y \times Z$ is determined by the final voxel grid size and C represents the channel count, adjustable according to the network. This tensor is progressively upscaled to the target voxel grid size. At each upscaling stage, the latent state $(\mathbf{s}_t, \mathbf{h}_t)$ is injected into the tensor \mathcal{T}_n (n denoting the tensor post- n upscaling stages) via adaptive instance normalization [49]. 3D occupancy representations can be directly used for downstream tasks in autonomous driving, such as semantic segmentation, object detection, or motion planning [22, 84, 89, 92, 127].

By customizing either the size of the kernel \mathcal{K} or the tensor \mathcal{T}_0 , both the 2D and 3D reconstruction approaches can be tailored to different output resolutions. Qualitative examples of our predictions can be found in Figure 3 and 7.

3.5. Training Losses

Our unsupervised world model is trained based on a typical sensor setup of autonomous vehicles [27, 109] with stereo cameras and lidar, requiring no labels and thus allowing for training on large fleet datasets. For each modality, we down-sample multiple times with ratios of 1, 2, and 4. With this multi-scale approach, we compute losses at different resolutions, reinforcing the network’s learning from the data.

- **Images:** We output RGB images that align with the size of the input image and utilize the common L1 loss \mathcal{L}^{img} for the minimization of the absolute discrepancies between target and prediction.
- **Point clouds:** We generate range view images of dimensions $H_r \times W_r \times 4$, which can be converted into $N \times 3$ point cloud data. The target is the range view image transformed from the ground truth, where an L2 loss $\mathcal{L}^{\text{p}, \text{xyz}}$ is applied to the (x, y, z) coordinates to minimize the Euler distance and an L1 loss $\mathcal{L}^{\text{p}, r}$ is based on range r .
- **3D Occupancy:** Voxel grids of size $192 \times 192 \times 64$ with $0.5m$ voxels, where each voxel contains the binary occupancy. The target is obtained by voxelizing fused depth maps from depth cameras and point clouds from lidar. The loss function combines cross-entropy $\mathcal{L}^{\text{v}, \text{ce}}$ with a Scene-Class Affinity Loss (SCAL) [8] $\mathcal{L}^{\text{v}, \text{scal}}$.

Combining these terms, the total loss is given by

$$\mathcal{L} = \sum \lambda_i (\lambda_{\text{img}} \mathcal{L}_i^{\text{img}} + \lambda_{\text{pcd}} (\mathcal{L}_i^{\text{p}, \text{xyz}} + \mathcal{L}_i^{\text{p}, r} + \mathcal{L}_i^{\text{pcd}}) + \lambda_{\text{v}} (\mathcal{L}_i^{\text{v}, \text{ce}} + \mathcal{L}_i^{\text{v}, \text{scal}})) \quad (2)$$

where i is the downsampling scale and λ denotes the weights balancing each loss term.

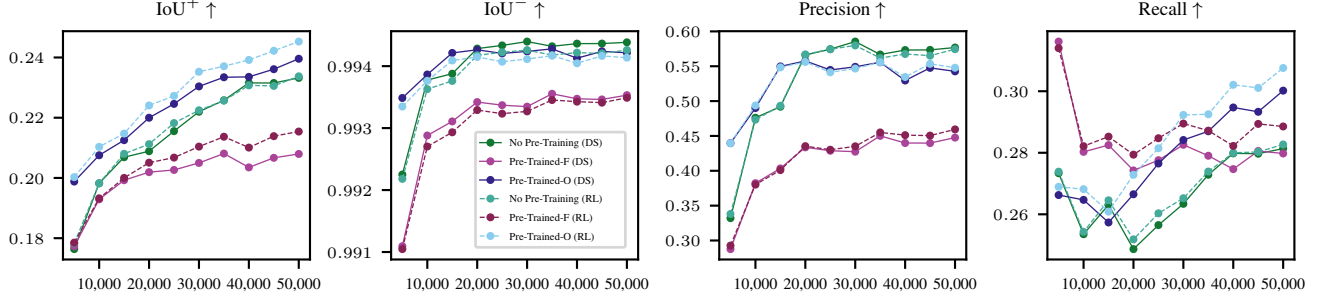


Figure 5. Evaluation of the influence of camera-lidar pre-training for 50,000 steps on 3D occupancy prediction. We evaluate on both \mathcal{D}_{val}^{RL} and \mathcal{D}_{val}^{DS} . The green lines show our benchmark without pre-training. The violet lines show experiments where the weights of the pre-trained model were frozen, while the weights remained open for the blue lines.

4. Experimental Settings

4.1. Dataset

Training Set. We collected our training dataset \mathcal{D}_{train} in the CARLA simulation environment [20] using an expert reinforcement learning agent [40, 131]. Our data collection encompasses four towns (Town01, Town03, Town04, Town06) and four weather conditions (Clear Noon, Wet Noon, Hard Rain Noon, Clear Sunset), gathered at a frequency of 10 FPS. For each town, we executed 25 runs, each lasting 300 seconds, with randomly selected weather conditions, amounting to 8.3 hours or 300,000 frames of data. For each frame, we save the RGB image $\mathcal{I} \in \mathbb{R}^{3 \times 600 \times 960}$, depth map $\mathcal{I}_D \in \mathbb{R}^{1 \times 600 \times 960}$, e.g., derived from stereo cameras, point cloud $\mathcal{P} \in \mathbb{R}^{\leq 60,000 \times 3}$ obtained from a lidar with 64 vertical channels, route map $\mathbf{route} \in \mathbb{R}^{1 \times 64 \times 64}$ as the planned route in BEV space, speed $\mathbf{v} \in \mathbb{R}$, and actions $\mathbf{a} \in \mathbb{R}^2$ in the form of acceleration and steering angle.

Validation Sets. To validate our model, we adopt the same setup as before but introduce variations to create two distinct validation sets. For each town, we execute five 300-second long driving sessions with the following settings:

- \mathcal{D}_{val}^{RL} : This set uses the same cities and weather conditions as the training set. However, the driving routes are randomized, thereby ensuring different routes from those in the training data. The primary goal is to evaluate the effectiveness of our model in representation learning (RL) in familiar environments.
- \mathcal{D}_{val}^{DS} : In this set, we maintain the same cities as in the training set but introduce different weather conditions (Soft Rain Sunset, Wet Sunset, Cloudy Noon, Mid Rain Sunset). Additionally, the driving routes are also randomized to ensure they differ from those in the training set. The introduction of this dataset is designed to evaluate the performance of our model when faced with a domain shift (DS), specifically assessing its generalization capabilities and robustness.

4.2. Training Parameters

For training, we sampled data from the training set at intervals of 0.2 seconds, creating sequences of length 12 to serve as training inputs. During training, all 12 frames were treated as known data. In the experiments containing voxel reconstructions, we reduced the length of sequences to 6 to speed up the training. We trained with a batch size of 16. We utilized the AdamW optimizer, with a learning rate of 10^{-4} and a weight decay of 0.01. During validation, we used 6/4 frames as given observations, while 6/2 served as ground truth for the predictions.

4.3. Metrics

To evaluate the performance of our model, we used different metrics based on the evaluated modality:

- **Camera.** For assessing the quality of image reconstructions, we used the Peak Signal-to-Noise Ratio (PSNR) as a common metric to assess average differences.
- **Lidar.** We used the Chamfer Distance to evaluate the accuracy of point cloud reconstructions, which measures the average closest point distance between two point clouds.
- **3D Occupancy.** For the reconstruction of voxel occupancy grids, we used the standard metrics Intersection over Union (IoU), Precision, and Recall. We differentiate between IoU^+ , which analyzes occupied voxels, and IoU^- , which evaluates empty voxels.

5. Evaluation

5.1. Sensor Fusion

To determine an optimal sensor fusion approach, we performed multiple ablation studies. In Sec. 5.1.1, we describe examined decoders and fusion methods not yet introduced. Subsequently, Sec. 5.1.2 provides an overview and a comparison of the analyzed combinations.

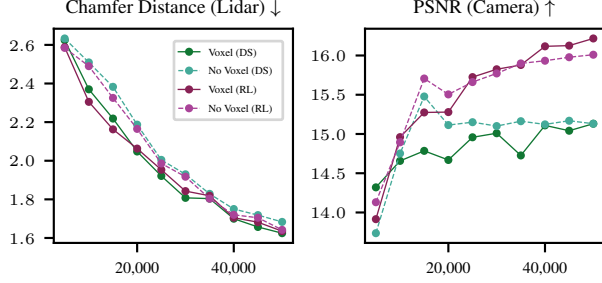


Figure 6. Impact of predicting 3D occupancy on the quality of camera and lidar predictions, evaluated on both \mathcal{D}_{val}^{RL} and \mathcal{D}_{val}^{DS} .

5.1.1 Encoders and Fusion Methods

Images. For the image features \mathcal{F}_c , we evaluate the already in Sec. 3 introduced encoder as well as the approach common in literature [40, 61] to map features to a BEV space [78]. First, features are elevated into a 3D space. Then, these 3D feature voxels are aggregated into the BEV space, leading to image features $\mathcal{F}_b \in \mathbb{R}^{C \times H_b \times W_b}$.

Point Clouds. Next to the range view-based approach described in Sec. 3.1, we also evaluate PointPillars [53] as an encoder. Here, point cloud data is segmented into discrete Pillars along the X and Y axes followed by data processing and feature extraction, resulting in a 2D pseudo-image $\mathcal{P}(u, v) \in \mathbb{R}^{C_p \times H_p \times W_p}$ from a BEV perspective.

Fusion Methods. Next to the transformer-based architecture described in Sec. 3, we explore naive combinations of the encoded 1D features from each sensor modality. We evaluate both a simple averaging of these features as well as concatenating them followed by a fully connected layer.

5.1.2 Model Architecture

We conducted experiments on the prediction performance of eight encoder-fusion combinations, as visible in Figure 4. We follow a naming scheme A-B-C:

- **A** represents the method of processing point clouds: **PP** stands for the use of PointPillars as the encoder; **RV** indicates the conversion of point clouds into range view representations, as shown in Sec. 3.1.
- **B** denotes the approach of image processing: **BEV** implies mapping to Bird’s Eye View followed by feature extraction with a ResNet-18; **RN** denotes that only a ResNet-18 is used for feature extraction from images.
- **C** describes the method of sensor fusion: **AVG** stands for the averaging of 1D features; **FC** means that concatenation followed by a fully connected layer is performed; **TR** denotes that the transformer-based multi-head self-attention mechanism was used, as described in Sec. 3.2.

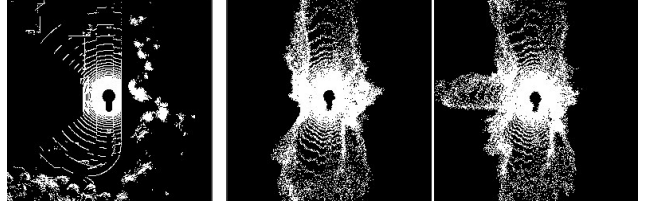


Figure 7. Diverse Predictions: The seed scenario on the left indicates that the agent might approach an intersection. MUVO can predict diverse, plausible futures, as shown on the right.

Image Prediction. The results of our ablation study for image predictions based on PSNR, where higher values mean better performance, can be found in Figure 4. When comparing the performance on different validation sets, we can observe a drop in performance for all networks in the \mathcal{D}_{val}^{DS} dataset, but the relative performance of different networks remains consistent across both datasets. In both cases, our transformer-based architecture (RV-RN-TR) performs on par or better compared to the other combinations. Generally speaking, range view-based lidar encodings show clear advantages over PointPillars. The additional BEV mapping of image features does not show any significant benefits in the image prediction task. We can see that the effectiveness of introducing a transformer-based architecture depends on the encoder used. It outperforms other approaches when combined with a ResNet-18 for feature extraction. In contrast, when combined with PP and BEV, its performance is lower than the FC but higher than AVG.

Point Cloud Prediction. Examining the Chamfer Distance plots in Figure 4, where lower values mean better performance, we find no significant performance disparity between both validation datasets. For \mathcal{D}_{val}^{RL} , our transformer-based architecture (RV-RN-TR) performs on par or better compared to the other combinations. However, on \mathcal{D}_{val}^{DS} , its performance drops. As before, range view-based methods demonstrate superiority over PointPillars. However, BEV shows no clear disadvantage for this task. We can see that transformer-based architectures generally outperform other fusion techniques for this task.

Based on these results, we employed the transformer-based architecture with range view representations for point clouds, as described in Sec. 3, since we are more interested in strong representations than in strong generalization capabilities of the model in the context of this work.

5.2. 3D Occupancy Prediction

For our 3D occupancy representation, we are interested in whether our occupancy model can benefit from a pre-trained model on camera and lidar data alone, since it is computationally much more efficient, and, in turn, if it can improve the predictions of camera and lidar data.



Figure 8. Observed failure cases: Top left shows a missing pedestrian in the prediction. Top right shows a reconstruction of a car into another car of the same class. Bottom left shows a strong blur. Bottom right shows a viewpoint mismatch.

5.2.1 Impact on 3D Occupancy Predictions

We perform experiments in three scenarios, as shown in Figure 5. We first trained a model - as a pre-trained starting point - with camera and lidar data alone for 50,000 steps.

- **Pre-Trained-Frozen (PTF).** We employ the pre-trained model but freeze all of its weights so that only the weights of the voxel decoder are trained. This approach allows us to assess the impact of fine-tuning only the voxel-specific aspects of the model while keeping the rest of the network, in particular all encoders, constant to evaluate if any information about a discrete geometry of the world is already encoded based on camera and lidar data alone.
- **Pre-Trained-Open (PTO).** The pre-trained weights were also used as a starting point, but the entire network was open for weight updates during training. This experiment enables us to analyze how the pre-trained weights influence the learning process when the whole network adapts and evolves during training.
- **No Pre-Training (NPT).** We train the network from scratch without utilizing any pre-trained weights. This benchmark enables us to determine whether pre-training weights only with images and point clouds contribute to better 3D occupancy predictions.

In Figure 5 we can see that the model trained from scratch (NPT) exhibits a similar performance on both validation datasets across all four metrics, while the other two models using pre-trained weights (PTF and PTO) generally performed better on \mathcal{D}_{val}^{RL} than on \mathcal{D}_{val}^{DS} across three metrics, excluding IoU^- . Interestingly, for IoU^- we observe an opposite behavior, where the models perform better on \mathcal{D}_{val}^{DS} . This is attributed to voxel occupancy grid predictions focus-

ing more on occupied grids. Since voxel grids are mostly empty, models on \mathcal{D}_{val}^{DS} tend to predict more noise, leading to lower IoU^- scores. Comparing PTO to NPT, the PTO model showed advantages early on, supporting the idea that pre-trained weights contribute valuable spatial knowledge. However, in the later stages of training, the NPT model overtook the PTO model in Precision, while in IoU^- and Recall the PTO model remained superior. This indicates that the non-pre-trained model adopts a more conservative strategy for 3D occupancy prediction. When we examine the PTF scenario, although the model underperformed compared to the other two, its performance improved over time by only training the voxel decoder. This improvement underscores that the pre-trained weights already contain some, however limited spatial information, indicating that the model partially integrates image and point cloud features to form spatial voxel features even when trained only on these two modalities.

5.2.2 Impact on Camera and Lidar Predictions

We perform a set of experiments to determine whether knowledge encoded through our occupancy approach can be leveraged by the lidar and camera prediction tasks, as shown in Figure 6. Based on the Chamfer Distance curve for point clouds and the PSNR curve for images, we can see slightly increased performance gains for both modalities, when voxel prediction is included.

6. Conclusion

Conclusion. We have presented MUVO, an unsupervised generative world model with Geometric Representations in the form of 3D occupancy voxels. Our approach leverages typical multimodal sensor setups of autonomous vehicles, processing raw, high-dimensional camera and lidar data. Our model is capable of predicting and decoding diverse and plausible high-resolution future observations. In addition, MUVO learns a sensor-agnostic 3D occupancy representation, leveraging geometric knowledge about the real world. Our predicted 3D occupancy grids can be directly used for downstream tasks, such as planning [22]. To the best of our knowledge, we are the first to demonstrate action-conditioned occupancy predictions. In addition, we showed that the geometrical representation improves both camera and lidar predictions.

Limitations and Outlook. As visible in Figure 3 and 8, our model still suffers from a set of failure cases, which can in part be attributed to our simulation environment. In future work, we want to scale up our unsupervised approach with real-world data collected by our research vehicles, leveraging larger and more diverse driving data.

References

- [1] Xuyang Bai, Zeyu Hu, Xinge Zhu, Qingqiu Huang, Yilun Chen, Hangbo Fu, and Chiew-Lan Tai. TransFusion: Robust LiDAR-Camera Fusion for 3D Object Detection with Transformers. In *CVPR*, 2022. 2
- [2] Philipp Becker and Gerhard Neumann. On Uncertainty in Deep State Space Models for Model-Based Reinforcement Learning. *Transactions on Machine Learning Research*, 2022. 1
- [3] J. Behley, M. Garbade, A. Milioto, J. Quenzel, S. Behnke, C. Stachniss, and J. Gall. SemanticKITTI: A Dataset for Semantic Scene Understanding of LiDAR Sequences. In *ICCV*, 2019. 2
- [4] Daniel Bogdoll, Lukas Bosch, Tim Joseph, Helen Gremmelmaier, Yitian Yang, and J. Marius Zöllner. Exploring the Potential of World Models for Anomaly Detection in Autonomous Driving. In *IEEE Symp. Comp. Intell.*, 2023. 1
- [5] Holger Caesar, Varun Bankiti, Alex H. Lang, Sourabh Vora, Venice Erin Liong, Qiang Xu, Anush Krishnan, Yu Pan, Giancarlo Baldan, and Oscar Beijbom. nuScenes: A Multimodal Dataset for Autonomous Driving. In *CVPR*, 2020. 2
- [6] Holger Caesar, Juraj Kabzan, Kok Seang Tan, Whye Kit Fong, Eric Wolff, Alex Lang, Luke Fletcher, Oscar Beijbom, and Sammy Omari. NuPlan: A closed-loop ML-based planning benchmark for autonomous vehicles. *arXiv:2106.11810*, 2022. 2
- [7] Qi Cai, Yingwei Pan, Ting Yao, Chong-Wah Ngo, and Tao Mei. ObjectFusion: Multi-modal 3D Object Detection with Object-Centric Fusion. In *ICCV*, 2023. 2
- [8] Anh-Quan Cao and Raoul De Charette. MonoScene: Monocular 3D Semantic Scene Completion. In *CVPR*, 2022. 2, 5
- [9] Anh-Quan Cao and Raoul de Charette. SceneRF: Self-Supervised Monocular 3D Scene Reconstruction with Radiance Fields. In *ICCV*, 2023. 2
- [10] Alexandra Carlson, Manikandasriram Srinivasan Ramanagopal, Nathan Tseng, Matthew Johnson-Roberson, Ram Vasudevan, and Katherine A. Skinner. CLONER: Camera-Lidar Fusion for Occupancy Grid-aided Neural Representations. *Rob. Aut. Lett.*, 8(5), 2023. 2
- [11] Jianyu Chen, Shengbo Eben Li, and Masayoshi Tomizuka. Interpretable End-to-End Urban Autonomous Driving With Latent Deep Reinforcement Learning. *IEEE Trans. Intell. Transp. Sys.*, 23, 2022. 5
- [12] Lili Chen, Kevin Lu, Aravind Rajeswaran, Kimin Lee, Aditya Grover, Michael Laskin, Pieter Abbeel, Aravind Srinivas, and Igor Mordatch. Decision Transformer: Reinforcement Learning via Sequence Modeling. *arXiv:2106.01345*, 2021. 2
- [13] Min Chen, Zhao Dawei, Xiao Liang, Nie Yiming, and Dai Bin. UniWorld: Autonomous Driving Pre-training via World Models. *arXiv:2308.07234*, 2023. 3
- [14] Xuanyao Chen, Tianyuan Zhang, Yue Wang, Yilun Wang, and Hang Zhao. FUTR3D: A Unified Sensor Fusion Framework for 3D Detection. In *CVPRW*, 2023. 2
- [15] Kashyap Chitta, Aditya Prakash, Bernhard Jaeger, Zehao Yu, Katrin Renz, and Andreas Geiger. TransFuser: Imitation with Transformer-Based Sensor Fusion for Autonomous Driving. *IEEE TPAMI*, 2022. 2, 3, 4, 5
- [16] Kyunghyun Cho, Bart van Merriënboer, Caglar Gulcehre, Dzmitry Bahdanau, Fethi Bougares, Holger Schwenk, and Yoshua Bengio. Learning Phrase Representations using RNN Encoder-Decoder for Statistical Machine Translation. *arXiv:1406.1078*, 2014. 4
- [17] comma.ai. CommaVQ: A dataset of tokenized driving video and a GPT model, 2023. 2
- [18] OpenScene Contributors. Openscene: The largest up-to-date 3d occupancy prediction benchmark in autonomous driving, 2023. 2
- [19] Jiajun Deng, Shaoshuai Shi, Peiwei Li, Wengang Zhou, Yanyong Zhang, and Houqiang Li. Voxel R-CNN: Towards High Performance Voxel-based 3D Object Detection. In *AAAI*, 2021. 2
- [20] Alexey Dosovitskiy, German Ros, Felipe Codevilla, Antonio Lopez, and Vladlen Koltun. CARLA: An open urban driving simulator. In *Conf. Rob. Learn.*, 2017. 6
- [21] Alexey Dosovitskiy, Lucas Beyer, Alexander Kolesnikov, Dirk Weissenborn, Xiaohua Zhai, Thomas Unterthiner, Mostafa Dehghani, Matthias Minderer, Georg Heigold, Sylvain Gelly, Jakob Uszkoreit, and Neil Houlsby. An Image is Worth 16x16 Words: Transformers for Image Recognition at Scale. In *ICLR*, 2020. 4
- [22] Ashok Elluswamy. Occupancy Networks. CVPR Workshop on Autonomous Driving, 2023. 2, 5, 8
- [23] Ashok Elluswamy. Foundation Models for Autonomy. CVPR Workshop on Autonomous Driving, 2023. 2
- [24] Lue Fan, Ziqi Pang, Tianyuan Zhang, Yu-Xiong Wang, Hang Zhao, Feng Wang, Naiyan Wang, and Zhaoxiang Zhang. Embracing Single Stride 3D Object Detector with Sparse Transformer. In *CVPR*, 2022. 2, 3
- [25] Stefano Ferraro, Pietro Mazzaglia, Tim Verbelen, and Bart Dhoedt. FOCUS: Object-Centric World Models for Robotics Manipulation. *arXiv:2307.02427*, 2023. 1
- [26] Zeyu Gao, Yao Mu, Ruoyan Shen, Chen Chen, Yangang Ren, Jianyu Chen, Shengbo Eben Li, Ping Luo, and Yanfeng Lu. Enhance Sample Efficiency and Robustness of End-to-end Urban Autonomous Driving via Semantic Masked World Model. In *NeurIPS*, 2022. 2, 4
- [27] Andreas Geiger, Philip Lenz, Christoph Stiller, and Raquel Urtasun. Vision meets robotics: The kitti dataset. *International Journal of Robotics Research (IJRR)*, 2013. 2, 3, 5
- [28] Benjamin Graham, Martin Engelcke, and Laurens Van Der Maaten. 3D Semantic Segmentation with Submanifold Sparse Convolutional Networks. In *CVPR*, 2018. 2
- [29] David Ha and Jürgen Schmidhuber. Recurrent world models facilitate policy evolution. In *NeurIPS*, 2018. 1, 5
- [30] Danijar Hafner, Timothy Lillicrap, Ian Fischer, Ruben Villegas, David Ha, Honglak Lee, and James Davidson. Learning Latent Dynamics for Planning from Pixels. In *Int. Conf. Mach. Learn.*, 2019. 1, 4

- [31] Danijar Hafner, Timothy Lillicrap, Jimmy Ba, and Mohammad Norouzi. Dream to Control: Learning Behaviors by Latent Imagination. In *ICLR*, 2020. 1, 4, 5
- [32] Danijar Hafner, Timothy Lillicrap, Mohammad Norouzi, and Jimmy Ba. Mastering Atari with Discrete World Models. In *ICLR*, 2021. 1, 2
- [33] Danijar Hafner, Jurgis Pasukonis, Jimmy Ba, and Timothy Lillicrap. Mastering Diverse Domains through World Models. *arXiv:2301.04104*, 2023. 2, 4
- [34] Nicklas Hansen, Xiaolong Wang, and Hao Su. Temporal Difference Learning for Model Predictive Control. In *Int. Conf. Mach. Learn.*, 2022. 1
- [35] Adrian Hayler, Felix Wimbauer, Dominik Muhle, Christian Rupprecht, and Daniel Cremers. S4C: Self-Supervised Semantic Scene Completion with Neural Fields. *arXiv:2310.07522*, 2023. 2
- [36] Kaiming He, Xiangyu Zhang, Shaoqing Ren, and Jian Sun. Deep Residual Learning for Image Recognition. In *CVPR*, 2016. 3, 5
- [37] Kaiming He, Xinlei Chen, Saining Xie, Yanghao Li, Piotr Dollar, and Ross Girshick. Masked Autoencoders Are Scalable Vision Learners. In *CVPR*, 2022. 2
- [38] Mikael Henaff, Alfredo Canziani, and Yann LeCun. Model-Predictive Policy Learning with Uncertainty Regularization for Driving in Dense Traffic. In *ICLR*, 2019. 1
- [39] Georg Hess, Johan Jaxing, Elias Svensson, David Hagerman, Christoffer Petersson, and Lennart Svensson. Masked Autoencoder for Self-Supervised Pre-training on Lidar Point Clouds. In *WACV*, 2023. 2
- [40] Anthony Hu, Gianluca Corrado, Nicolas Griffiths, Zak Murez, Corina Gurau, Hudson Yeo, Alex Kendall, Roberto Cipolla, and Jamie Shotton. Model-Based Imitation Learning for Urban Driving. In *NeurIPS*, 2022. 1, 2, 3, 4, 5, 6, 7
- [41] Anthony Hu, Lloyd Russell, Hudson Yeo, Zak Murez, George Fedoseev, Alex Kendall, Jamie Shotton, and Gianluca Corrado. GAIA-1: A Generative World Model for Autonomous Driving. *arXiv:2309.17080*, 2023. 1, 2, 4
- [42] Jordan S. K. Hu, Tianshu Kuai, and Steven L. Waslander. Point Density-Aware Voxels for LiDAR 3D Object Detection. In *CVPR*, 2022. 2
- [43] Keli Huang, Botian Shi, Xiang Li, Xin Li, Siyuan Huang, and Yikang Li. Multi-modal Sensor Fusion for Auto Driving Perception: A Survey. *arXiv:2202.02703*, 2022. 2
- [44] Yuanhui Huang, Wenzhao Zheng, Yunpeng Zhang, Jie Zhou, and Jiwen Lu. Tri-Perspective View for Vision-Based 3D Semantic Occupancy Prediction. In *CVPR*, 2023. 2
- [45] Michael Janner, Qiyang Li, and Sergey Levine. Offline Reinforcement Learning as One Big Sequence Modeling Problem. In *NeurIPS*, 2021. 2
- [46] Xiaosong Jia, Penghao Wu, Li Chen, Jiangwei Xie, Conghui He, Junchi Yan, and Hongyang Li. Think Twice before Driving: Towards Scalable Decoders for End-to-End Autonomous Driving. In *CVPR*, 2023. 2
- [47] Haoyi Jiang, Tianheng Cheng, Naiyu Gao, Haoyang Zhang, Wenyu Liu, and Xinggang Wang. Symphonize 3D Semantic Scene Completion with Contextual Instance Queries. *arXiv:2306.15670*, 2023. 2
- [48] Lukasz Kaiser, Mohammad Babaeizadeh, Piotr Milos, Blazej Osinski, Roy H. Campbell, Konrad Czechowski, Dumitru Erhan, Chelsea Finn, Piotr Kozakowski, Sergey Levine, Afroz Mohiuddin, Ryan Sepassi, George Tucker, and Henryk Michalewski. Model-Based Reinforcement Learning for Atari. In *ICLR*, 2020. 1
- [49] Tero Karras, Samuli Laine, and Timo Aila. A style-based generator architecture for generative adversarial networks. In *CVPR*, 2019. 5
- [50] Tarasha Khurana, Peiyun Hu, David Held, and Deva Ramanan. Point Cloud Forecasting as a Proxy for 4D Occupancy Forecasting. In *CVPR*, 2023. 2, 5
- [51] Seung Wook Kim, Yuhao Zhou, Jonah Philion, Antonio Torralba, and Sanja Fidler. Learning to Simulate Dynamic Environments with GameGAN. In *CVPR*, 2020. 1
- [52] Seung Wook Kim, , Jonah Philion, Antonio Torralba, and Sanja Fidler. DriveGAN: Towards a Controllable High-Quality Neural Simulation. In *CVPR*, 2021. 2
- [53] Alex H. Lang, Sourabh Vora, Holger Caesar, Lubing Zhou, Jiong Yang, and Oscar Beijbom. PointPillars: Fast Encoders for Object Detection From Point Clouds. In *CVPR*, 2019. 2, 5, 7
- [54] Yann LeCun. A Path Towards Autonomous Machine Intelligence. *OpenReview:BZ5a1r-kVsf*, 2022. 1
- [55] Bo Li, Tianlei Zhang, and Tian Xia. Vehicle Detection from 3D Lidar Using Fully Convolutional Network. *arXiv:1608.07916*, 2016. 5
- [56] Xin Li, Tao Ma, Yuenan Hou, Botian Shi, Yuchen Yang, Youquan Liu, Xingjiao Wu, Qin Chen, Yikang Li, Yu Qiao, and Liang He. LoGoNet: Towards Accurate 3D Object Detection with Local-to-Global Cross-Modal Fusion. In *CVPR*, 2023. 2
- [57] Yanwei Li, Yilun Chen, Xiaojuan Qi, Zeming Li, Jian Sun, and Jiaya Jia. Unifying Voxel-based Representation with Transformer for 3D Object Detection. In *NeurIPS*, 2022. 2
- [58] Yiming Li, Sihang Li, Xinhao Liu, Moonjun Gong, Kenan Li, Nuo Chen, Zijun Wang, Zhiheng Li, Tao Jiang, Fisher Yu, Yue Wang, Hang Zhao, Zhiding Yu, and Chen Feng. SSCBench: Monocular 3D Semantic Scene Completion Benchmark in Street Views. *arXiv:2306.09001*, 2023. 2
- [59] Yiming Li, Zhiding Yu, Christopher Choy, Chaowei Xiao, Jose M Alvarez, Sanja Fidler, Chen Feng, and Anima Anandkumar. Voxformer: Sparse voxel transformer for camera-based 3d semantic scene completion. In *CVPR*, 2023. 2
- [60] Zhiqi Li, Zhiding Yu, David Austin, Mingsheng Fang, Shiyi Lan, Jan Kautz, and Jose M. Alvarez. FB-OCC: 3D Occupancy Prediction based on Forward-Backward View Transformation. In *CVPRW*, 2023. 2
- [61] Tingting Liang, Hongwei Xie, Kaicheng Yu, Zhongyu Xia, Zhiwei Lin, Yongtao Wang, Tao Tang, Bing Wang, and Zhi Tang. BEVFusion: A Simple and Robust LiDAR-Camera Fusion Framework. In *NeurIPS*, 2022. 2, 7
- [62] Yiyi Liao, Jun Xie, and Andreas Geiger. KITTI-360: A Novel Dataset and Benchmarks for Urban Scene Understanding in 2D and 3D. *IEEE TPAMI*, 2022. 2

- [63] Fangchen Liu, Hao Liu, Aditya Grover, and Pieter Abbeel. Masked Autoencoding for Scalable and Generalizable Decision Making. In *NeurIPS*, 2023. 2
- [64] Haisong Liu, Tao Lu, Yihui Xu, Jia Liu, Wenjie Li, and Lijun Chen. CamLiFlow: Bidirectional Camera-LiDAR Fusion for Joint Optical Flow and Scene Flow Estimation. In *CVPR*, 2022. 2
- [65] Xinhao Liu, Moonjun Gong, Qi Fang, Haoyu Xie, Yiming Li, Hang Zhao, and Chen Feng. LiDAR-based 4D Occupancy Completion and Forecasting. *arXiv:2310.11239*, 2023. 2, 3, 5
- [66] Zhijian Liu, Haotian Tang, Alexander Amini, Xinyu Yang, Huizi Mao, Daniela L. Rus, and Song Han. BEVFusion: Multi-Task Multi-Sensor Fusion with Unified Bird’s-Eye View Representation. In *ICRA*, 2023. 2
- [67] Yunze Man, Liang-Yan Gui, and Yu-Xiong Wang. BEV-Guided Multi-Modality Fusion for Driving Perception. In *CVPR*, 2023. 2
- [68] Jiageng Mao, Yujing Xue, Minzhe Niu, Haoyue Bai, Jiashi Feng, Xiaodan Liang, Hang Xu, and Chunjing Xu. Voxel Transformer for 3D Object Detection. In *ICCV*, 2021. 2
- [69] Russell Mendonca, Shikhar Bahl, and Deepak Pathak. Structured World Models from Human Videos. In *Rob. Sci. Sys.*, 2023. 2
- [70] Ruihang Miao, Weizhou Liu, Mingrui Chen, Zheng Gong, Weixin Xu, Chen Hu, and Shuchang Zhou. OccDepth: A Depth-Aware Method for 3D Semantic Scene Completion. *arXiv:2302.13540*, 2023. 2
- [71] Vincent Micheli, Eloi Alonso, and François Fleuret. Transformers are Sample-Efficient World Models. In *ICLR*, 2022. 2
- [72] Chen Min, Liang Xiao, Dawei Zhao, Yiming Nie, and Bin Dai. UniScene: Multi-Camera Unified Pre-training via 3D Scene Reconstruction. *arXiv:2305.18829*, 2023. 2
- [73] Chen Min, Xinli Xu, Dawei Zhao, Liang Xiao, Yiming Nie, and Bin Dai. Occupancy-MAE: Self-supervised Pre-training Large-scale LiDAR Point Clouds with Masked Occupancy Autoencoders. *arXiv:2206.09900*, 2023. 2
- [74] Minting Pan, Xiangming Zhu, Yunbo Wang, and Xiaokang Yang. Iso-Dream: Isolating and Leveraging Noncontrollable Visual Dynamics in World Models. In *NeurIPS*, 2022. 1
- [75] Mingjie Pan, Jiaming Liu, Renrui Zhang, Peixiang Huang, Xiaoqi Li, Li Liu, and Shanghang Zhang. RenderOcc: Vision-Centric 3D Occupancy Prediction with 2D Rendering Supervision. *arXiv:2309.09502*, 2023. 2
- [76] Mingjie Pan, Li Liu, Jiaming Liu, Peixiang Huang, Longlong Wang, Shanghang Zhang, Shaoqing Xu, Zhiyi Lai, and Kuiyuan Yang. UniOcc: Unifying Vision-Centric 3D Occupancy Prediction with Geometric and Semantic Rendering. In *CVPRW*, 2023. 2
- [77] Su Pang, Daniel Morris, and Hayder Radha. Fast-CLOCs: Fast Camera-LiDAR Object Candidates Fusion for 3D Object Detection. In *WACV*, 2022. 2
- [78] Jonah Philion and Sanja Fidler. Lift, Splat, Shoot: Encoding Images from Arbitrary Camera Rigs by Implicitly Unprojecting to 3D. In *ECCV*, 2020. 2, 5, 7
- [79] Yiran Qin, Chaoqun Wang, Zijian Kang, Ningning Ma, Zhen Li, and Ruimao Zhang. SupFusion: Supervised LiDAR-Camera Fusion for 3D Object Detection. In *ICCV*, 2023. 2
- [80] Alec Radford, Jong Wook Kim, Chris Hallacy, Aditya Ramesh, Gabriel Goh, Sandhini Agarwal, Girish Sastry, Amanda Askell, Pamela Mishkin, Jack Clark, Gretchen Krueger, and Ilya Sutskever. Learning Transferable Visual Models From Natural Language Supervision. In *Int. Conf. Mach. Learn.*, 2021. 2
- [81] Scott Reed, Konrad Zolna, Emilio Parisotto, Sergio Gomez Colmenarejo, Alexander Novikov, Gabriel Barth-Maron, Mai Gimenez, Yury Sulsky, Jackie Kay, Jost Tobias Springenberg, Tom Eccles, Jake Bruce, Ali Razavi, Ashley Edwards, Nicolas Heess, Yutian Chen, Raia Hadsell, Oriol Vinyals, Mahyar Bordbar, and Nando de Freitas. A Generalist Agent. In *Trans. Mach. Learn. Research*, 2022. 2
- [82] Christoph B. Rist, David Emmerichs, Markus Enzweiler, and Dariu M. Gavrilă. Semantic Scene Completion using Local Deep Implicit Functions on LiDAR Data. In *IEEE TPAMI*, 2021. 2
- [83] Robin Rombach, Andreas Blattmann, Dominik Lorenz, Patrick Esser, and Björn Ommer. High-Resolution Image Synthesis with Latent Diffusion Models. *arXiv:2112.10752*, 2022. 2
- [84] Danila Rukhovich, Anna Vorontsova, and Anton Konushin. ImVoxelNet: Image to Voxels Projection for Monocular and Multi-View General-Purpose 3D Object Detection. In *WACV*, 2022. 5
- [85] Younggyo Seo, Danijar Hafner, Hao Liu, Fangchen Liu, Stephen James, Kimin Lee, and Pieter Abbeel. Masked World Models for Visual Control. In *Conf. Rob. Learn.*, 2023. 1
- [86] Hao Shao, Letian Wang, RuoBing Chen, Hongsheng Li, and Yu Liu. Safety-Enhanced Autonomous Driving Using Interpretable Sensor Fusion Transformer. In *Conf. Rob. Learn.*, 2022. 2, 4
- [87] Shaoshuai Shi, Chaoxu Guo, Li Jiang, Zhe Wang, Jianping Shi, Xiaogang Wang, and Hongsheng Li. PV-RCNN: Point-Voxel Feature Set Abstraction for 3D Object Detection. In *CVPR*, 2020. 2
- [88] Shaoshuai Shi, Li Jiang, Jiajun Deng, Zhe Wang, Chaoxu Guo, Jianping Shi, Xiaogang Wang, and Hongsheng Li. PV-RCNN++: Point-Voxel Feature Set Abstraction With Local Vector Representation for 3D Object Detection. *IJCV*, 131(2), 2023. 2
- [89] Yining Shi, Kun Jiang, Jiusi Li, Junze Wen, Zelin Qian, Mengmeng Yang, Ke Wang, and Diange Yang. Grid-Centric Traffic Scenario Perception for Autonomous Driving: A Comprehensive Review. *arXiv:2303.01212*, 2023. 5
- [90] Elena Shrestha, Chetan Reddy, Hanxi Wan, Yulun Zhuang, and Ram Vasudevan. Sense, Imagine, Act: Multimodal Perception Improves Model-Based Reinforcement Learning for Head-to-Head Autonomous Racing. *arXiv:2305.04750*, 2023. 1, 3, 4
- [91] Oren Shtrout, Yizhak Ben-Shabat, and Ayellet Tal. GraVoS:

- Voxel Selection for 3D Point-Cloud Detection. In *CVPR*, 2023. 2
- [92] Chonghao Sima, Wenwen Tong, Tai Wang, Li Chen, Silei Wu, Hanming Deng, Yi Gu, Lewei Lu, Ping Luo, Dahua Lin, and Hongyang Li. Scene as occupancy. In *ICCV*, 2023. 2, 5
- [93] Shuran Song, Fisher Yu, Andy Zeng, Angel X. Chang, Manolis Savva, and Thomas Funkhouser. Semantic Scene Completion from a Single Depth Image. In *CVPR*, 2017. 2
- [94] Pei Sun, Henrik Kretschmar, Xerxes Dotiwalla, Aurelien Chouard, Vijaysai Patnaik, Paul Tsui, James Guo, Yin Zhou, Yuning Chai, Benjamin Caine, Vijay Vasudevan, Wei Han, Jiquan Ngiam, Hang Zhao, Aleksei Timofeev, Scott Ettinger, Maxim Krivokon, Amy Gao, Aditya Joshi, Yu Zhang, Jonathon Shlens, Zhifeng Chen, and Dragomir Anguelov. Scalability in perception for autonomous driving: Waymo open dataset. In *CVPR*, 2020. 2
- [95] Zhiyu Tan, Zichao Dong, Cheng Zhang, Weikun Zhang, Hang Ji, and Hao Li. OVO: Open-Vocabulary Occupancy. *arXiv:2305.16133*, 2023. 2
- [96] Haotian Tang, Zhijian Liu, Shengyu Zhao, Yujun Lin, Ji Lin, Hanrui Wang, and Song Han. Searching Efficient 3D Architectures with Sparse Point-Voxel Convolution. In *ECCV*, 2020. 2
- [97] Josh Tenenbaum. Learning to see the human way. Keynote at CVPR, 2022. 3
- [98] Xiaoyu Tian, Tao Jiang, Longfei Yun, Yue Wang, Yilun Wang, and Hang Zhao. Occ3d: A large-scale 3d occupancy prediction benchmark for autonomous driving. *arXiv:2304.14365*, 2023. 2
- [99] Aaron van den Oord, Oriol Vinyals, and koray kavukcuoglu. Neural Discrete Representation Learning. In *NeurIPS*, 2017. 2
- [100] Ashish Vaswani, Noam Shazeer, Niki Parmar, Jakob Uszkoreit, Llion Jones, Aidan N Gomez, Łukasz Kaiser, and Illia Polosukhin. Attention is All you Need. In *NeurIPS*, 2017. 2, 4
- [101] Antonin Vobecky, Oriane Siméoni, David Hurych, Spyros Gidaris, Andrei Bursuc, Patrick Pérez, and Josef Sivic. POP-3D: Open-Vocabulary 3D Occupancy Prediction from Images. In *NeurIPS*, 2023. 2
- [102] Thang Vu, Jung-Hee Kim, Myeongjin Kim, Seokwoo Jung, and Seong-Gyun Jeong. MiLO: Multi-task Learning with Localization Ambiguity Suppression for Occupancy Prediction. In *CVPRW*, 2023. 2
- [103] Zhexiong Wan, Yuxin Mao, Jing Zhang, and Yuchao Dai. RPEFlow: Multimodal Fusion of RGB-PointCloud-Event for Joint Optical Flow and Scene Flow Estimation. In *ICCV*, 2023. 2
- [104] Haiyang Wang, Chen Shi, Shaoshuai Shi, Meng Lei, Sen Wang, Di He, Bernt Schiele, and Liwei Wang. DSVT: Dynamic Sparse Voxel Transformer with Rotated Sets. In *CVPR*, 2023. 2
- [105] Tai Wang, Xinge Zhu, and Dahua Lin. Reconfigurable Voxels: A New Representation for LiDAR-Based Point Clouds. In *Conf. Rob. Learn.*, 2021. 2
- [106] Xiaofeng Wang, Zheng Zhu, Guan Huang, Xinze Chen, and Jiwen Lu. DriveDreamer: Towards Real-world-driven World Models for Autonomous Driving. *arXiv:2309.09777*, 2023. 2
- [107] Xiaofeng Wang, Zheng Zhu, Wenbo Xu, Yunpeng Zhang, Yi Wei, Xu Chi, Yun Ye, Dalong Du, Jiwen Lu, and Xingang Wang. Openoccupancy: A large scale benchmark for surrounding semantic occupancy perception. *arXiv:2303.03991*, 2023. 2
- [108] Yuqi Wang, Yuntao Chen, Xingyu Liao, Lue Fan, and Zhaoxiang Zhang. PanoOcc: Unified Occupancy Representation for Camera-based 3D Panoptic Segmentation. *arXiv:2306.10013*, 2023. 2
- [109] Waymo. Introducing the 5th-generation waymo driver, 2020. 3, 5
- [110] Yi Wei, Linqing Zhao, Wenzhao Zheng, Zheng Zhu, Jie Zhou, and Jiwen Lu. SurroundOcc: Multi-Camera 3D Occupancy Prediction for Autonomous Driving. In *ICCV*, 2023. 2
- [111] Felix Wimbauer, Nan Yang, Christian Rupprecht, and Daniel Cremers. Behind the Scenes: Density Fields for Single View Reconstruction. In *CVPR*, 2023. 2
- [112] Philipp Wu, Alejandro Escontrela, Danijar Hafner, Ken Goldberg, and Pieter Abbeel. Daydreamer: World models for physical robot learning. *Conf. Rob. Learn.*, 2022. 2, 3, 4, 5
- [113] Philipp Wu, Arjun Majumdar, Kevin Stone, Yixin Lin, Igor Mordatch, Pieter Abbeel, and Aravind Rajeswaran. Masked trajectory models for prediction, representation, and control. In *International Conference on Machine Learning*, 2023. 2
- [114] Pengchuan Xiao, Zhenlei Shao, Steven Hao, Zishuo Zhang, Xiaolin Chai, Judy Jiao, Zesong Li, Jian Wu, Kai Sun, Kun Jiang, Yunlong Wang, and Diange Yang. PandaSet: Advanced Sensor Suite Dataset for Autonomous Driving. In *IEEE Intell. Transp. Syst. Conf.*, 2021. 2
- [115] Yichen Xie, Chenfeng Xu, Marie-Julie Rakotosaona, Patrick Rim, Federico Tombari, Kurt Keutzer, Masayoshi Tomizuka, and Wei Zhan. SparseFusion: Fusing Multi-Modal Sparse Representations for Multi-Sensor 3D Object Detection. In *ICCV*, 2023. 2
- [116] Jianyun Xu, Ruixiang Zhang, Jian Dou, Yushi Zhu, Jie Sun, and Shiliang Pu. RPNNet: A Deep and Efficient Range-Point-Voxel Fusion Network for LiDAR Point Cloud Segmentation. In *ICCV*, 2021. 2
- [117] Runsen Xu, Tai Wang, Wenwei Zhang, Runjian Chen, Jinkun Cao, Jiangmiao Pang, and Dahua Lin. MV-JAR: Masked Voxel Jigsaw and Reconstruction for LiDAR-Based Self-Supervised Pre-Training. In *CVPR*, 2023. 2
- [118] Junjie Yan, Yingfei Liu, Jianjian Sun, Fan Jia, Shuailin Li, Tiancai Wang, and Xiangyu Zhang. Cross Modal Transformer: Towards Fast and Robust 3D Object Detection. In *ICCV*, 2023. 2
- [119] Xu Yan, Jiantao Gao, Jie Li, Ruimao Zhang, Zhen Li, Rui Huang, and Shuguang Cui. Sparse Single Sweep LiDAR Point Cloud Segmentation via Learning Contextual Shape Priors from Scene Completion. In *AAAI*, 2020. 2

- [120] Xiangchao Yan, Runjian Chen, Bo Zhang, Jiakang Yuan, Xinyu Cai, Botian Shi, Wenqi Shao, Junchi Yan, Ping Luo, and Yu Qiao. SPOT: Scalable 3D Pre-training via Occupancy Prediction for Autonomous Driving, 2023. 2
- [121] Yan Yan, Yuxing Mao, and Bo Li. SECOND: Sparsely Embedded Convolutional Detection. *Sensors*, 18, 2018. 2
- [122] Honghui Yang, Wenxiao Wang, Minghao Chen, Binbin Lin, Tong He, Hua Chen, Xiaofei He, and Wanli Ouyang. PVT-SSD: Single-Stage 3D Object Detector with Point-Voxel Transformer. In *CVPR*, 2023. 2
- [123] Honghui Yang, Sha Zhang, Di Huang, Xiaoyang Wu, Haoyi Zhu, Tong He, Shixiang Tang, Hengshuang Zhao, Qibo Qiu, Binbin Lin, Xiaofei He, and Wanli Ouyang. UniPAD: A Universal Pre-training Paradigm for Autonomous Driving, 2023. 2
- [124] Zeyu Yang, Jiaqi Chen, Zhenwei Miao, Wei Li, Xiatian Zhu, and Li Zhang. DeepInteraction: 3D Object Detection via Modality Interaction. In *NeurIPS*, 2022. 2
- [125] Maosheng Ye, Shuangjie Xu, and Tongyi Cao. HVNet: Hybrid Voxel Network for LiDAR Based 3D Object Detection. In *CVPR*, 2020. 2
- [126] Tianwei Yin, Xingyi Zhou, and Philipp Krahenbuhl. Center-based 3D Object Detection and Tracking. In *CVPR*, 2021. 2
- [127] Wenyuan Zeng, Wenjie Luo, Simon Suo, Abbas Sadat, Bin Yang, Sergio Casas, and Raquel Urtasun. End-to-end Interpretable Neural Motion Planner, 2019. 5
- [128] Yihan Zeng, Da Zhang, Chunwei Wang, Zhenwei Miao, Ting Liu, Xin Zhan, Dayang Hao, and Chao Ma. LIFT: Learning 4D LiDAR Image Fusion Transformer for 3D Object Detection. In *CVPR*, 2022. 2
- [129] Lunjun Zhang, Yuwen Xiong, Ze Yang, Sergio Casas, Rui Hu, and Raquel Urtasun. Learning Unsupervised World Models for Autonomous Driving via Discrete Diffusion. *arXiv:2311.01017*, 2023. 2, 4
- [130] Yunpeng Zhang, Zheng Zhu, and Dalong Du. OccFormer: Dual-path Transformer for Vision-based 3D Semantic Occupancy Prediction, 2023. 2
- [131] Zhejun Zhang, Alexander Liniger, Dengxin Dai, Fisher Yu, and Luc Van Gool. End-to-end urban driving by imitating a reinforcement learning coach. In *ICCV*, 2021. 6
- [132] Zhejun Zhang, Alexander Liniger, Dengxin Dai, Fisher Yu, and Luc Van Gool. Trafficbots: Towards world models for autonomous driving simulation and motion prediction. In *International Conference on Robotics and Automation (ICRA)*, 2023. 2
- [133] Zhiwei Zhang, Zhizhong Zhang, Qian Yu, Ran Yi, Yuan Xie, and Lizhuang Ma. LiDAR-Camera Panoptic Segmentation via Geometry-Consistent and Semantic-Aware Alignment. In *ICCV*, 2023. 2
- [134] Yin Zhou and Oncel Tuzel. VoxelNet: End-to-End Learning for Point Cloud Based 3D Object Detection. In *CVPR*, 2018. 2
- [135] Benjin Zhu, Zhengkai Jiang, Xiangxin Zhou, Zeming Li, and Gang Yu. Class-balanced Grouping and Sampling for Point Cloud 3D Object Detection. In *CVPRW*, 2019. 2
- [136] Benjin Zhu, Zhe Wang, Shaoshuai Shi, Hang Xu, Lanqing Hong, and Hongsheng Li. ConQueR: Query Contrast Voxel-DETR for 3D Object Detection. In *CVPR*, 2023. 2